Generation of Arbitrary Quadrature Signals Using One Dual-Drive Modulator

Keang-Po Ho, *Senior Member, IEEE,* and Han-Wei Cuei

***Abstract*—Regardless of the number of constellation points, all quadrature-amplitude modulation (QAM) signals can be generated using a single dual-drive Mach–Zehnder modulator. When the general method is applied to quadrature-phase-shift-keying (QPSK) signals, three different QPSK transmitters are shown with drive signals having four, three, or two levels. The usage of only one dual-drive modulator greatly simplifies the design of QAM and QPSK transmitters.**

***Index Terms*—Differential quadrature phase-shift keying (DQPSK), external modulator, quadrature amplitude modulation, spectral efficiency.**

I. Introduction

RECENTLY, multilevel modulation signals like differential quadrature phase-shift keying (DQPSK) have received renewed attention to improve the spectral efficiency of a lightwave communication system [1]–[9]. Those demonstrations of DQPSK signals usually have a spectral efficiency more than 1 b/s/Hz. One of the recent demonstrations by [9] achieves a distance of 6400 km for 64 channels of a 12.5-Gb/s DQPSK data stream. The spectral efficiency can be up to 2.5 b/s/Hz for system with polarization multiplexing [6], [7].

Other than the requirement of a precoder [1], [10], the transmitters of DQPSK signals and quadrature-phase-shift-keying (QPSK) signals are basically the same. The previous implementation of DQPSK transmitters of [1], [2], [5]–[7], and [11] is shown in Fig. 1. Not only for (D)QPSK signals, but also for the general class of quadrature-amplitude modulation (QAM) with and without differential operation, the transmitter of Fig. 1 is the usual method to generate a QAM signal using two Mach–Zehnder modulators (MZMs) within two $\pi/2$-phase difference paths of a Mach–Zehnder interferometer. The transmitter of Fig. 1 is the direct implementation of the quadrature transmitter in a standard digital communication textbook [12, Fig. 7.27].

Intuitively, the two MZMs of Fig. 1 generate the signal for the two quadrature components with a phase difference of $\pi/2$, i.e., cosine and sine. If the two normalized drive signals of the transmitter of Fig. 1 are a and b, respectively, the baseband complex representation of the output of the transmitter is the complex number of $a + be^{-j\pi/2} = a - bj$. The two MZMs of Fig. 1 must operate with a peak-to-peak drive voltage of $2V_\pi$ such that both a and b can be both positive and negative values with minimum signal loss. The output electric field is thus

$$E_o = \Re\{(a - bj)e^{\omega_c t}\} = a\cos(\omega_c t) + b\sin(\omega_c t) \quad (1)$$

where $\Re\{\cdot\}$ denotes the real part of a complex number and ω_c is the angular frequency of the optical carrier. The representation of (1) is the same as conventional representation from [12, eq. (7.113)] with a and b from two independent drive signals of the two MZMs in Fig. 1.

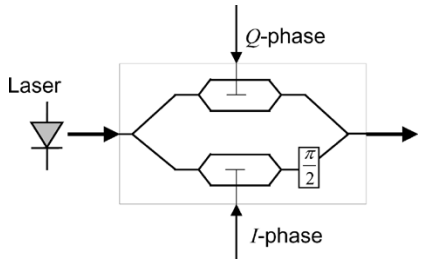

Fig. 1. QAM transmitter based on two MZMs in an interferometer.

With two MZMs and an interferometer, the special modulator of Fig. 1 is difficult to fabricate. If the transmitter of Fig. 1 is implemented using discrete components of two MZMs within an interferometer, the transmitter is costly with many components. The transmitter in Fig. 1 also requires two bias controls for the MZMs and a phase control of the $\pi/2$ phase shifter. As shown subsequently, the QAM signal can also be generated using a single dual-drive MZM. When the technique is applied to (D)QPSK signals, three different transmitters are invented with a drive signal having four, three, and two levels, respectively. The usage of only one dual-drive MZM greatly simplifies the design of the (D)QPSK transmitter.

The remainder of this paper is organized as follows. Section II provides the general principle for the generation of the QAM signal using a single dual-drive MZM. Section III is the application of the technique to (D)QPSK signals with three different implementations of a (D)QPSK transmitter. Section IV is the conclusion of the paper.

II. General Principles

Fig. 2 is the basic structure of a dual-drive MZM. The dual-drive MZM consists of two phase modulators that can be operated independently.

The MZM can be fabricated using various materials [13]–[19], and $LiNbO_3$ is the most popular material [13],

Manuscript received May 14, 2004; revised September 1, 2004. This research was supported in part by the National Science Council (NSC) of Taiwan under Grants NSC-93-2213-E-002-061, NSC-93-2219-E-002-007, and NSC-93-2219-E-002-008

K.-P. Ho is with the Institute of Communication Engineering and Department of Electrical Engineering, National Taiwan University, Taipei 106, Taiwan, R.O.C. (e-mail: kpho@cc.ee.ntu.edu.tw).

H.-W. Cuei is with the Institute of Communication Engineering, National Taiwan University, Taipei 106, Taiwan, R.O.C.

Digital Object Identifier 10.1109/JLT.2004.838855

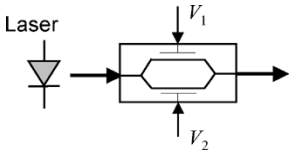

Fig. 2. Basic structure of a dual-drive MZM with two independent phase modulators in a Mach–Zehnder interferometer.

[15]. Almost all commercial long-haul dense-wavelength-division-multiplexed (DWDM) systems use $LiNbO_3$ MZM. In the dual-drive structure of Fig. 2, the modulator chirp is adjustable [20], [21]. Currently, a dual-drive 40-Gb/s modulator with a V_π of less than 2 V has been demonstrated experimentally [22].

Assumed steady-state operation for simplicity, if the two paths of a dual-drive MZM have independent drive voltages of V_1 and V_2, with an input electric field of E_i, the output electric field is

$$E_o = \frac{E_i}{2}\left[\exp\left(j\pi\frac{V_1}{V_\pi}\right) + \exp\left(j\pi\frac{V_2}{V_\pi}\right)\right] \tag{2}$$

where V_π is the voltage to provide a π phase shift of each phase modulator. In the most trivial case, the MZM is operated as a phase modulator if $V_1 = V_2$. By choosing both V_1 and V_2 of (2) properly, any quadrature signal can be generated. The input and output relationship of (2) is rewritten in the normalized form of

$$E_o = \frac{r_{\max}}{2}\left(e^{j\phi_1} - e^{j\phi_2}\right) \tag{3}$$

where $\phi_1 = \pi V_1/V_\pi$ and $\phi_2 = \pi V_2/V_\pi + \pi$. The output electric field of E_o is the difference of two vectors in the circle having a radius of $(1/2)r_{\max}$. The MZM of (3) is biased at the minimum transmission point or the null point, and the maximum output electric field has an amplitude of $r_{\max}$ when $V_1 = V_2$ or ϕ_1 and ϕ_2 are antipodal phases. The representation of (3) gives a simple geometric representation of the operation of a dual-drive MZM with two independent phase modulators.

Assume an M-ary signal constellation that can be represented as complex numbers of

$$s_i = r_i e^{j\theta_i}, \quad r_i > 0, \quad 0 \le \theta_i < 2\pi, \quad i = 0, \ldots, M-1 \tag{4}$$

with a maximum amplitude of

$$r_{\max} = \max\{r_0, r_1, \ldots, r_{M-1}\}. \tag{5}$$

With two phases of [23], [24]

$$\phi_{i1} = \theta_i + \cos^{-1}\left(\frac{r_i}{r_{\max}}\right) \tag{6}$$

$$\phi_{i2} = \theta_i - \cos^{-1}\left(\frac{r_i}{r_{\max}}\right) + \pi \tag{7}$$

we obtain

$$s_i = \frac{r_{\max}}{2}\left(e^{j\phi_{i1}} - e^{j\phi_{i2}}\right). \tag{8}$$

Fig. 3 shows the procedure to find the two phases of ϕ_{i1} and ϕ_{i2} in the circle with radius of $(1/2)r_{\max}$ for the constellation point of s_i. The real number of r_i is equal to the sum of two

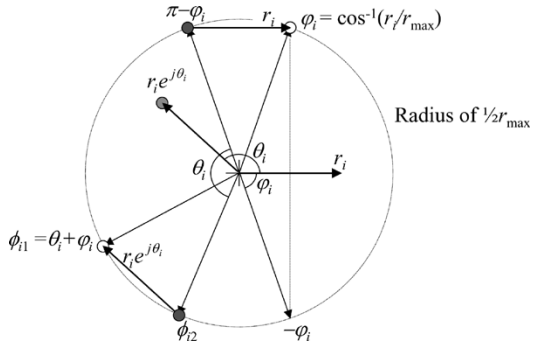

Fig. 3. Procedure to find ϕ_{i1} and ϕ_{i2} for $s_i = r_i e^{j\theta_i}$.

conjugated symmetrical complex numbers of $(1/2)r_i \pm jy_i$ in the circle with a radius of $(1/2)r_{\max}$, i.e., $(1/4)r_i^2 + y_i^2 = (1/4)r_{\max}^2$. With $\varphi_i = \cos^{-1}(r_i/r_{\max})$, we obtain $(1/2)r_i \pm jy_i = (1/2)r_{\max}e^{\pm j\varphi_i}$. Fig. 3 represents the two complex numbers of $(1/2)r_{\max}e^{\pm j\varphi_i}$ as two vectors with phase angles of $\pm\varphi_i$. The real number of r_i is given by $r_i = (1/2)r_{\max}e^{j\varphi_i} + (1/2)r_{\max}e^{-j\varphi_i}$. Alternatively, we may rewrite the summation as the difference of

$$r_i = \frac{1}{2}r_{\max}e^{j\varphi_i} - \frac{1}{2}r_{\max}e^{j(\pi-\varphi_i)}. \tag{9}$$

Fig. 3 also shows the difference of (9) to find r_i. The signal of $s_i = r_i e^{j\theta_i}$ is a rotation of θ_i from r_i. If $e^{j\theta_i}$ is multiple to both sides of (9), we obtain the expression of (8) with ϕ_{i1} and ϕ_{i2} given by (6) and (7), respectively. In Fig. 3, the three vectors of r_i, $(1/2)r_{\max}e^{j\varphi_i}$, and $(1/2)r_{\max}e^{j(\pi-\varphi_i)}$ are rotated by an angle of θ_i to obtain $r_i e^{j\theta_i}$, $(1/2)r_{\max}e^{j\phi_{i1}}$, and $(1/2)r_{\max}e^{j\phi_{i2}}$, respectively.

All constellation points of (4) can be generated based on two phase modulators having the phases of (6) and (7), respectively. QAM signals or arbitrary quadrature signals are separated into two phase-modulated signals by [23] and [24]. These types of linear amplification using nonlinear components (LINC) transmitters are very popular in wireless communications [25]–[27]. The two phases of (6) and (7) drive the two phase modulators of Fig. 2 of the dual-drive MZM.

Fig. 4 shows a 16-QAM constellation and the phases of (6) and (7) for the dual-drive MZM to generate the constellation. Instead of representing all 16 constellation points in the same figure, Fig. 4(a) separates the 16-QAM signal into two QPSK and one 8-PSK signals. Fig. 4(b)–(d) shows the corresponding ϕ_{i1} and ϕ_{i2} of all 16 points according to the separation of Fig. 4(a). The empty and solid circles represent ϕ_{i1} and ϕ_{i2}, respectively. Fig. 4(b) gives the QPSK signal of Fig. 4(a) with a maximum amplitude of $r_{\max}$. For illustration purpose, the two closest points of Fig. 4(b) are the same but drawn differently for the phases of two different signals. Fig. 4(c) generates the 8-PSK signal of Fig. 4(a). Fig. 4(d) gives the QPSK signal of Fig. 4(a) with the smallest amplitude.

From Fig. 4, the generation of a 16-QAM signal using a dual-drive MZM requires the usage of a 16-level drive voltage and thus very complicated drive circuits. In the transmitter of Fig. 1, the two drive signals are two independent four-level drive signals corresponding to the x and y axis of Fig. 4(a). Compared with the conventional transmitter of Fig. 1, the simplification

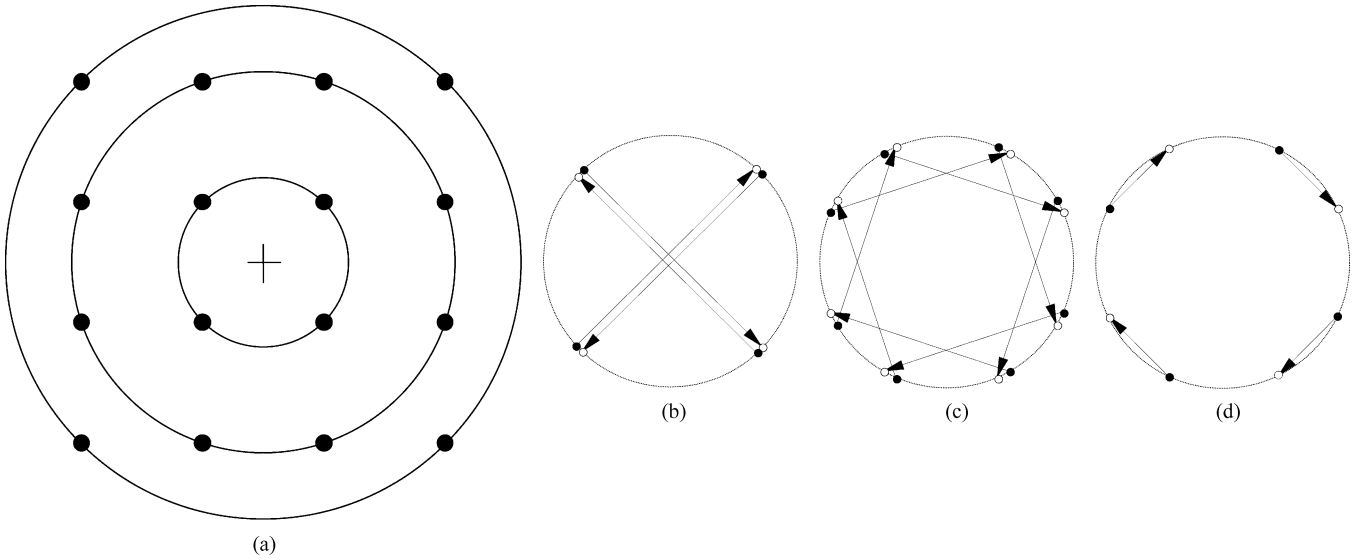

Fig. 4. (a) 16-QAM constellation and its separation into two QPSK signals and one 8-PSK signal. (b), (c), and (d) are the two phases of ϕ_1 (empty circles) and ϕ_2 (solid circles) to generate the 16-QAM signal. (a) 16-QAM. (b) Big QPSK. (c) 8-PSK. (d) Small QPSK.

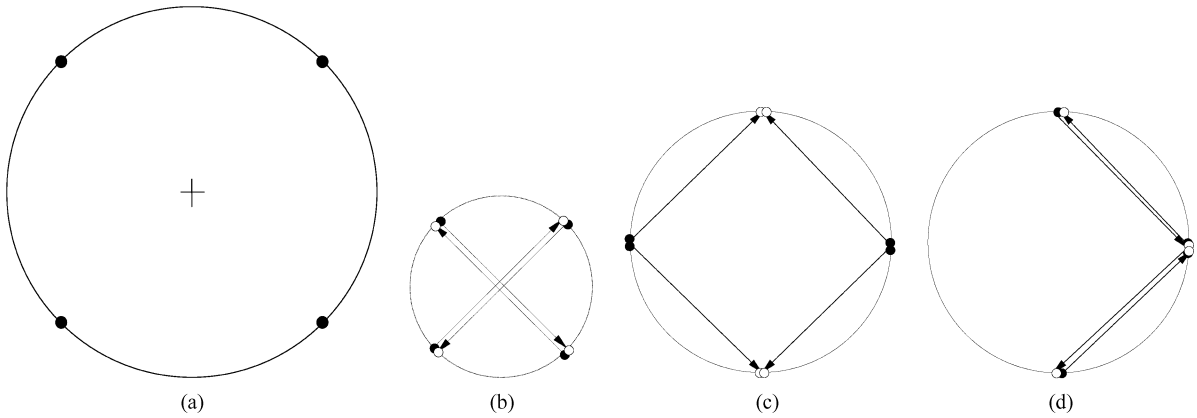

Fig. 5. (a) (D)QPSK constellation and its generation using dual-drive MZM with a (b) four-, (c) two-, and (d) three-drive-level signal. (a) (D)QPSK. (b) Four-level. (c) Two-level. (d) Three-level.

of the optical components using a single dual-drive MZM increases the complexity in the electronic circuits. With the allowance of higher modulator loss, as shown subsequently, the number of drive levels can be reduced.

III. Generation of (D)QPSK Signals

Currently, most spectral efficiency systems use DQPSK signals. The direct application of the signal separation method of (6) and (7) gives the trivial case of operating the dual-drive MZM as a phase modulator driven by a four-level signal. Practical applications of the dual-drive MZM require the reduction of the number of levels in the drive signal.

The dual-drive MZM transmitter of Fig. 2 can be used to generate (D)QPSK signals with a constellation of Fig. 5(a). Similar to that of Figs. 4(b) and 5(b) is the trivial case of operating the dual-drive MZM as a phase modulator when ϕ_1 and ϕ_2 are antipodal phases. The four phases of Fig. 5(a) are generated by a four-level drive signal. In [3], [4], [8], and [9], DQPSK signals are generated by the cascade of practically two phase modulators driven by two binary sequences. The usage of a dual-drive MZM as a phase modulator may not be an application that is of interest.

A (D)QPSK signal may be generated with higher loss but smaller number of levels if the four constellation points are generated with phases of ϕ_1 or ϕ_2 the same as one another. With only two values of ϕ_1 and ϕ_2, Fig. 5(c) drives the dual-drive MZM in Fig. 2 with a two-level drive signal. Fig. 5(d) has three different values of ϕ_1 and ϕ_2 and requires a three-level drive signal. In Fig. 5(c) and (d), all phases of ϕ_1 and ϕ_2 are located in a circle with the same diameter, representing the phase modulator with the same input signals. In Fig. 5(b)–(d), the vectors representing the output electric fields all have the same magnitude. The diameter of the circle of Fig. 5(b) is about $1/\sqrt{2}$ that of the circles of Fig. 5(c) and (d), requiring one half the power at the input of the dual-drive MZM to generate an output electric field of the same length. In other words, the schemes using a two- and three-level drive signal have 3-dB extra loss more than that of Fig. 5(b).

The peak-to-peak drive voltages of the two phase modulators in Fig. 2 are proportional to the maximum phase difference of ϕ_1 or ϕ_2, respectively. The maximum phase difference of the four

drive levels of Fig. 5(b) is $3\pi/2$ and that of the two and three drive levels of Fig. 5(c) and (d) is π. Both the peak-to-peak drive voltage and the number of drive levels are reduced in Fig. 5(c) and (d).

Fig. 5(b)–(d) shows the operation of the (D)QPSK transmitter in steady state when both ϕ_1 and ϕ_2 are in the correct phase angles. However, when the phases are in transition from one to another between consecutive transmitted symbols, the dynamic of the transmitter requires careful studies. Similar to the conventional transmitter of Fig. 1, both the two- and three-level transmitters of Fig. 5(c) and (d) do not have constant intensity between consecutive symbols. Fig. 6 shows a return-to-zero (RZ)-(D)QPSK transmitter with the assumption of the usage of a dual-drive MZM followed by an RZ modulator. In practice, the RZ modulator can either precede or follow the (D)QPSK generator. Without the RZ modulator, the transmitter of Fig. 6 gives a nonreturn-to-zero (NRZ)-(D)QPSK signal. The conventional transmitter of Fig. 1 can also be used in Fig. 6 to generate the (D)QPSK signals. The RZ modulator should be operated in the interval when the (D)QPSK signal generator is in steady state of Fig. 5(b)–(d). Regardless of the transmitter types to generate the (D)QPSK signal, after the RZ modulator, the optical intensity is ideally a constant pulse train without ripple between symbols. However, the output signal of the dual-drive MZM may have either overshoot and undershoot ripples.

Fig. 7 show the eye diagram of the drive signal and the optical intensity between the RZ modulator and the (D)QPSK transmitter. Fig. 7(a) is the eye diagram when the conventional transmitter of Fig. 1 is used with two two-level drive signals having a peak-to-peak drive voltage of $2V_\pi$. Using the dual-drive transmitter of Fig. 2, the peak-to-peak drive voltage is reduced from $1.5V_\pi$ for a four-level signal to V_π for two- and three-level drive signals.

The output intensity of the conventional transmitter has optical intensity ripples between consecutive symbols. With two or three levels of drive signal, the output intensity of the dual-drive MZM also has ripples between consecutive symbols. The simplest two-level scheme of Figs. 5(c) and 7(c) has overshoot ripples doubling the output intensity. The ripple of the three-level signal of Fig. 7(d) with a dual-drive transmitter is similar to that of Fig. 7(a) with a conventional transmitter. If the RZ modulator is operated in the middle of the eye diagram of Fig. 7, the ripples are cancelled, and the transmitter provides a constant pulse train. For an NRZ signal without an RZ modulator, overshoot ripples are equivalent to short optical pulses that are particularly detrimental and potentially give high signal distortion due to fiber nonlinearities. Without the RZ modulator, the two-level drive signals of Fig. 5(c) cannot be used for NRZ signals due to the overshoot ripples.

While Fig. 7 shows the eye diagram of the optical intensity, Fig. 8 shows the trace of the output electric field with both the real and imaginary parts. The four signal constellation points of Fig. 5(a) are shown in Fig. 8 as solid circles. The electric field of Fig. 8 other than the four signal constellation points occurs during the transition between consecutive (D)QPSK symbols. Other than Fig. 8(b) with all electric field in the same circle with equal distance to the origin (constant intensity), other traces show the electric field has a wide range of variations. Those

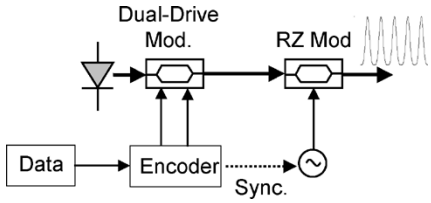

Fig. 6. RZ-(D)QPSK transmitter with a dual-drive MZM followed by an RZ modulator.

variations of electric field are equivalent to frequency chirp [20], [28].

In the conventional transmitter of Fig. 8(a), the electric field may pass through the origin and has an intensity equal to zero as shown in the optical intensity of Fig. 7(a). The electric field trace of the two-level signal of Figs. 5(c) and 7(c) shows a peak electric field about $\sqrt{2}$ of the steady-state amplitude, corresponding to optical intensity ripples twice the steady-state intensity. The trace for the three-level drive signal of Fig. 8(d) has the same behavior as Fig. 8(a). Of course, Fig. 8(d) has transition with constant intensity, but all transitions of the conventional signal of Fig. 8(a) have ripples.

When the RZ modulator is used to convert the signal into a pulse train in Fig. 6, the electrical drive signal of Fig. 7 must have a short rise–fall time such that the signal transition is outside the RZ pulses. Because of the overshoot ripples, the two-level transmitter of Figs. 5(c) and 7(c) requires the shortest rise–fall time from the electrical drive signal. Assuming that the RZ modulator generates an RZ pulse with a duty-cycle of 50%, Fig. 9 shows the transmitted pulses when the 10%–90% rise–fall time of the electrical drive signal is $t_r = 0.2T$, $0.3T$, and $0.4T$. If the rise–fall time is 20% the symbol interval, there is insignificant signal distortion due to the overshoot of Fig. 7(c). Even for a rise–fall time approaching 40% of the bit interval, the ripples in the RZ pulses are below half of the peak intensity. Note that the ripples of the pulses of three- and four-level transmitters are less than that in Fig. 9.

The eye diagram of the received signal at the DQPSK receiver is also shown in Fig. 9 when the rise–fall time is equal to 40% of the symbol interval with $t_r = 0.4T$. The received signal of Fig. 9 is the output of a balanced receiver after an interferometer without phase error. Fig. 9 is for the in-phase branch of the DQPSK receiver, but that for the quadrature phase has no difference with Fig. 9. One of the purposes of Fig. 9 is to illustrate that the eye diagram of the transmitted intensity is similar to the upper half of the eye diagram of the received signal when the two-level transmitter is used. Practical systems may have shorter rise–fall times than $t_r = 0.4T$, but a longer rise–fall time of Fig. 9 is used to show the similarity between the eye diagrams of the intensity and received signal.

The ripples of the drive signal transfer to the optical signal. With the conventional transmitter of Fig. 1, no amplitude ripple of the drive signal transfers to the phase ripple. Even when the drive signal has a large ripple, the intensity ripple of the transmitted signal is compressed by the nonlinear transfer function of the MZM. For the (D)QPSK signal of Figs. 5 and 7, the ripples from the drive signal may be increased by the transmitter. Fig. 10 illustrates the increase of eye spreading when two

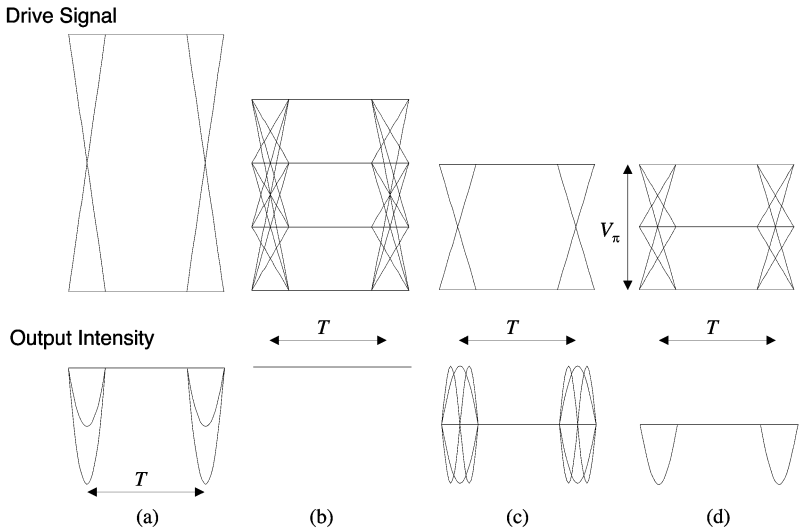

Fig. 7. Eye diagram of the drive signal and output intensity between two modulators of the transmitter of Fig. 6 when (a) the conventional transmitter of Fig. 1 and the dual-drive transmitter of Fig. 2 with (b) four-, (c) two-, and (d) three-level drive signals are used.

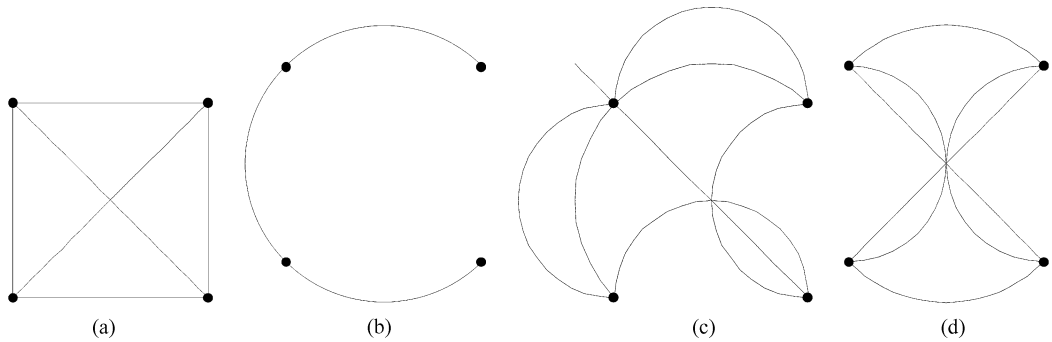

Fig. 8. Electric field locus of a (D)QPSK signal generated using (a) conventional transmitter of Fig. 1, and dual-drive transmitter of Fig. 2 with (b) four-, (c) two-, and (d) three-level drive signals. (a) Conventional. (b) Four-level. (c) Two-level. (d) Three-level.

two-level signals are summed to a four-level signal, for example, in the four-level transmitter of Fig. 5(b). If the eye spreading is defined as $\Delta_e = (\delta_1 + \delta_1)/d$, where δ_1 and δ_2 are the ripple (or spreading) in the upper and lower level, and d is the high of the eye diagram, the eye closure is $1 - (1/2)\Delta_e$ and the eye penalty is equal to $10 \cdot \log_{10}(1 - (1/2)\Delta_e)$. From Fig. 10, when two two-level signals of Fig. 10(a) and (b) are summed to the four-level signal of Fig. 10(c), the eye spreading is increased by a factor of three.

Table I shows the eye spreading of Δ_e for all RZ-DQPSK transmitters discussed in this paper and the conventional transmitter by assuming an "initial" eye spreading of 10% for convenience. In the four-level transmitter, the initial 10% eye spreading is increased to 30%, as illustrate in Fig. 10. For QPSK signals without the differential operation, the spreading of the received signal is also equal to 30%. When the dual-drive MZM functions as a phase modulator, the RZ pulses at the output of the transmitter do not have eye spreading, but the DQPSK receivers have an eye spreading of 47% due to phase distortion. The two-level transmitter provides a received signal spreading of about 32%, less than that of the four-level transmitter. The internal operation of the two-level transmitter may be similar to the illustration of Fig. 10. For the three-level transmitter, the eye spreading is increased by a factor of 1.5. In conventional transmitter, ripples of the drive signal do not transfer to phase ripple but only small amplitude ripple. Table I shows that a drive signal ripple of 10% gives a received signal ripples less than 1%.

For the DQPSK transmitter using dual-drive MZM, the eye spreading of the received signal increases almost linearly with the eye spreading of the drive signal. For an eye penalty of less than 1 dB at the received signal, 41% eye spreading is allowed, translating to a maximum eye spreading of the two-level signal of 8.7% and 12.8% for four- and two-level transmitters, respectively. For an eye penalty of less than 0.5 dB, 22% eye spreading is allowed, translating to a maximum eye spreading of the two-level signal of 5.7% and 6.9% for four- and two-level transmitters, respectively.

DQPSK signals can be demodulated by two interferometers corresponding to the phase difference of the DQPSK signals of Fig. 5 in consecutive symbols. To eliminate error propagation effects, DQPSK systems require a precoder [1], [10]. Without going into detail, the precoder for the two-level transmitter is equal to

$$\begin{aligned} p_k &= \overline{a_k \oplus b_k} \cdot \overline{b_k \oplus p_{k-1}} + (a_k \oplus b_k) \cdot \overline{b_k \oplus q_{k-1}} \\ q_k &= \overline{a_k \oplus b_k} \cdot \overline{b_k \oplus q_{k-1}} + (a_k \oplus b_k) \cdot (b_k \oplus p_{k-1}) \end{aligned} \quad (10)$$

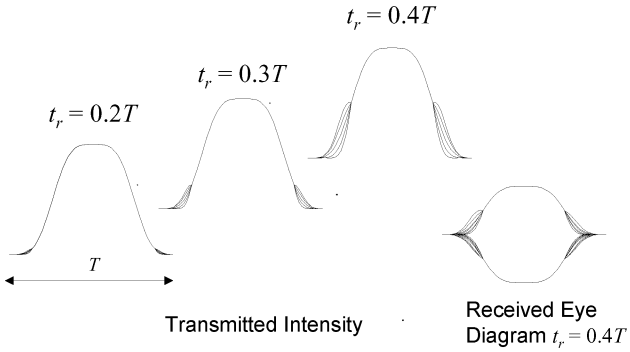

Fig. 9. Intensity of the optical pulse trains for the two-level (D)QPSK transmitter with a drive signal rise–fall time of $t_r = 0.2T$, $0.3T$, and $0.4T$.

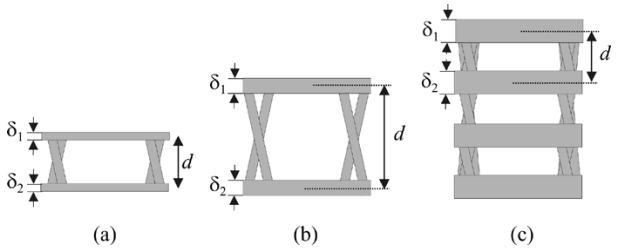

Fig. 10. Increases of eye spreading for a multilevel signal.

TABLE I
TRANSFER OF EYE SPREADING FROM DRIVE SIGNAL TO THE RECEIVER FOR DQPSK SIGNALS

Schemes	Two-Level	Multi-Level	RZ Pulses	Received Signal
Four-Level	10%	30%	1.3%	47%
Two-Level	10%	Nil	31%	33%
Three-Level	Nil	10%	15%	16%
Conventional	10%	Nil	0.7%	0.6%

where $\oplus$ denotes an exclusive-OR operation, a_k and b_k are the two input sequences to the precoder, and p_k and q_k are the two output sequences of the precoder. With less than ten logic gates, the precoder of (10) is similar to that in [10] and depends on the mapping of bits to phase differences and bits to symbols.

As long as the electrical drive signal has very good quality and the RZ modulator is used, the RZ-(D)QPSK transmitter using dual-drive MZM can generate mathematically the same signal as the conventional transmitter. The RZ-(D)QPSK signal broadens the bandwidth of the signal inversely proportional to the duty-cycle of the RZ pulses. Ripples or eye spreading transferred from the electrical drive signal are the major degradation using a phase modulator or dual-drive MZM to generate (D)QPSK signals.

IV. CONCLUSION

Similar to LINC in wireless communications [23]–[27], arbitrary QAM signals can be generated by two independent phase modulators that are the basic structure of a dual-drive MZM. A geometry representation is provided to give a simple illustration of the proposed signal decomposition scheme. Based on the geometry representation, the signal separation of a 16-QAM constellation is shown as an example.

To reduce the number of levels in the drive signals, in addition to the direct application of LINC to (D)QPSK signal, two dual-drive MZM-based transmitters are proposed with a drive signal having two and three levels. Similar to the conventional transmitter, the transmitters using two- and three-level drive signals have ripples between consecutive symbols. With an RZ modulator following or preceding the (D)QPSK generator, the ripples do not affect the performance of the RZ signal. For the NRZ signal without the RZ modulator, the (D)QPSK transmitter with a two-level drive signal has overshoot ripple twice the steady-state intensity.

REFERENCES

[1] R. A. Griffin, R. I. Johnston e, R. G. Walker, J. Hall, S. D. Wadsworth, K. Berry, A. C. Carter, M. J. Wale, P. A. Jerram, and N. J. Parsons, "10 Gb/s optical differential quadrature phase shift key (DQPSK) transmission using GaAs/AlGaAs integration," presented at the Optical Fiber Communication Conf. (OFC 2002), Anaheim, CA, 2002, Postdeadline Paper FD6.

[2] P. S. Cho, V. S. Grigoryan, Y. A. Godin, A. Salamon, and Y. Achiam, "Transmission of 25-Gb/s RZ-DQPSK signals with 25-GHz channel spacing over 1000 km of SMF-28 fiber," *IEEE Photon. Technol. Lett.*, vol. 15, no. 3, pp. 473–475, Mar. 2003.

[3] H. Kim and R.-J. Essiambre, "Transmission of 8 × 20 Gb/s DQPSK signals over 310-km SMF with 0.8 b/s/Hz spectral efficiency," *IEEE Photon. Technol. Lett.*, vol. 15, no. 5, pp. 769–771, May 2003.

[4] C. Wree, N. Hecker-Denschlag, E. Gottwald, P. Krummrich, J. Leibrich, E.-D. Schmidt, and B. L. W. Rosenkranz, "High spectral efficiency 1.6-b/s/Hz transmission (8 × 40 Gb/s with a 25-GHz grid) over 200-km SSMF using RZ-DQPSK and polarization multiplexing," *IEEE Photon. Technol. Lett.*, vol. 15, no. 9, pp. 1303–1305, Sep. 2003.

[5] Y. Zhu, K. Cordina, N. Jolley, R. Feced, H. Kee, R. Rickard, and A. Hadjifotiou, "1.6 bit/s/Hz orthogonally polarized CSRZ – DQPSK transmission of 8 × 40 Gbit/s over 320 km NDSF," presented at the Optical Fiber Communication Conf. (OFC 2004), Los Angeles, CA, 2004, Paper TuF1.

[6] P. S. Cho, G. Harston, C. J. Kerr, A. S. Greenblatt, A. Kaplan, Y. Achiam, G. Levy-Yurista, M. Margalit, Y. Gross, and J. B. Khurgin, "Investigation of 2-b/s/Hz 40-Gb/s DWDM transmission over 4 × 100 km SMF-28 fiber using RZ-DQPSK and polarization multiplexing," *IEEE Photon. Technol. Lett.*, vol. 16, no. 2, pp. 656–658, Feb. 2004.

[7] P. S. Cho, Y. Achiam, G. Levy-Yurista, M. Margalit, Y. Gross, and J. B. Khurgin, "Investigation of SOA nonlinearities on the amplification of DWDM channels with spectral efficiency up to 2.5 b/s/Hz," *IEEE Photon. Technol. Lett.*, vol. 16, no. 3, pp. 918–920, Mar. 2004.

[8] N. Yoshikane and I. Morita, "1.14 b/s/Hz spectrally-efficient 50 × 85.4 Gb/s transmission over 300 km using copolarized CS-RZ DQPSK signals," presented at the Optical Fiber Communication Conf. (OFC 2004), Los Angeles, CA, 2004, Postdeadline Paper PDP38.

[9] T. Tokle, C. R. Davidson, M. Nissov, J.-X. Cai, D. Foursa, and A. Pilipetskii, "6500 km transmission of RZ-DQPSK WDM signals," *Electron. Lett.*, vol. 40, no. 7, pp. 444–445, 2004.

[10] R. A. Griffin and A. C. Carter, "Optical differential quadrature phase-shift key (oDQPSK) for high capacity optical transmission," presented at the Optical Fiber Communication Conf. (OFC 2002), Anaheim, CA, 2002, Paper WX6.

[11] R. Griffin, R. Johnstone, R. Walker, S. Wadsworth, A. Carter, and M. Wale, "Integrated DQPSK transmitter for dispersion-tolerant and dispersion-managed DWDM transmission," presented at the Optical Fiber Communication Conf. (OFC 2003), Atlanta, GA, 2003, Paper FP6.

[12] S. Haykin, *Digital Communications*. New York: Wiley, 1988.

[13] R. C. Alferness, "Titanium-diffused lithium niobate waveguide devices," in *Guided-Wave Optoelectronics*, 2 ed, T. Tamir, Ed. Berlin, Germany: Springer-Verlag, 1990, pp. 145–210.

[14] W. K. Burns, M. M. Howerton, R. P. Moeller, R. R. Krähenbühl, R. W. McElhanon, and A. S. Greenblatt, "Low drive voltage, broad-band $LiNbO_3$ modulators with and without etched ridges," *J. Lightw. Technol.*, vol. 17, no. 12, pp. 2551–2555, Dec. 1999.

[15] E. L. Wooten, K. M. Kissa, A. Yi-Yan, E. J. Murphy, D. A. Lafaw, P. F. Hallemeier, D. Maack, D. V. Attanasio, D. J. Fritz, G. J. McBrien, and D. E. Bossi, "A review of lithium niobate modulators for fiber-optic communications systems," *IEEE J. Sel. Topics Quantum Electron.*, vol. 6, no. 1, pp. 69–82, Jan.–Feb. 2000.

[16] R. G. Walker, "High-speed electrooptic modulation in GaAs/GaAlAs waveguide devices," *J. Lightw. Technol.*, vol. LT-5, no. 10, pp. 1444–1453, Oct. 1987.

[17] F. J. Leonberger and J. P. Donnelly, "Semiconductor integrated optic devices," in *Guided-Wave Optoelectronics*, 2 ed, T. Tamir, Ed. Berlin, Germany: Springer-Verlag, 1990, pp. 317–396.

[18] Y. Shi, C. Zhang, H. Zhang, J. H. Bechtel, L. R. Dalton, B. H. Robinson, and W. H. Steier, "Low (sub-1-Volt) halfwave voltage polymeric electro-optic modulator achieved controlling chromophore shape," *Science*, vol. 288, pp. 119–122, 2000.

[19] A. Liu, R. Jones, L. Liao, D. Samara-Rubio, D. Rubin, O. Cohen, R. Nicolaescu, and M. Paniccia, "A high-speed silicon optical modulator based on a metal semiconductor capacitor," *Nature*, vol. 427, pp. 615–618, 2004.

[20] A. H. Gnauck, S. K. Korotky, J. J. Veselka, J. Nagel, C. T. Kemmerer, W. J. Minford, and D. T. Moser, "Dispersion penalty reduction using an optical modulator with adjustable chirp," *IEEE Photon. Technol. Lett.*, vol. 3, no. 10, pp. 916–918, Oct. 1991.

[21] K.-P. Ho and J. M. Kahn, "Spectrum of externally modulated optical signals," *J. Lightw. Technol.*, vol. 22, no. 2, pp. 658–663, Feb. 2004.

[22] M. Sugiyama, M. Doi, S. Taniguchi, T. Nakazawa, and H. Onaka, "Driver-less 40 Gb/s $LiNbO_3$ modulator with sub-1 V drive voltage," presented at the Optical Fiber Communication Conf. (OFC 2002), Anaheim, CA, 2002, Postdeadline Paper FB6.

[23] D. C. Cox, "Linear amplification with nonlinear components," *IEEE Trans. Commun.*, vol. COM-22, no. 12, pp. 1942–1945, Dec. 1974.

[24] D. C. Cox and R. P. Leck, "Component signal separation and recombination for linear amplification with nonlinear components," *IEEE Trans. Commun.*, vol. COM-23, no. 11, pp. 1281–1287, Nov. 1975.

[25] F. J. Casadevall and A. Valdovinos, "Performance analysis of QAM modulations applied to the LINC transmitter," *IEEE Trans. Veh. Technol.*, vol. 42, no. 4, pp. 399–406, 1993.

[26] B. Shi and L. Sundstrom, "A 200-MHz IF BiCMOS signal component separator for linear LINC transmitters," *IEEE J. Solid-State Circuits*, vol. 35, no. 7, pp. 987–993, Jul. 2000.

[27] X. Zhang, L. E. Larson, P. M. Asbeck, and P. Nanawa, "Gain/phase imbalance-minimization techniques for LINC transmitters," *IEEE Trans. Microwave Theory Tech.*, vol. 49, no. 12, pp. 2507–2516, Dec. 2001.

[28] F. Koyama and K. Oga, "Frequency chirping in external modulators," *J. Lightw. Technol.*, vol. 6, no. 1, pp. 87–93, Jan. 1988.

Keang-Po Ho (S'91–M'95–SM'03) received the B.S. degree from National Taiwan University, Taipei, Taiwan, R.O.C., in 1991 and the M.S. and Ph.D. degrees from the University of California at Berkeley in 1993 and 1995, respectively, all in electrical engineering.

He conducted research in the IBM T. J. Watson Research Center, Hawthorne, NY, on all-optical networks in the summer of 1994. He was a Research Scientist with Bellcore, currently Telcordia Technologies, Red Bank, NJ, from 1995 to 1997, where he conducted research on optical networking, high-speed lightwave systems, and broad-band access. He taught in the Department of Information Engineering of the Chinese University of Hong Kong, Hong Kong, from 1997 to 2001. He served as the Chief Technology Officer of StrataLight Communications, Campbell, CA, from 2000 to 2003, where he developed spectrally efficiency 40-Gb/s lightwave transmission systems. He has been with the Institute of Communication Engineering and Department of Electrical Engineering, National Taiwan University, since 2003. He has published more than 70 journal articles and has given numerous conference presentation on those fields. His research interests include optical communication systems, multimedia communication systems, combined source-channel coding, and communication theory. He was among the pioneers for research on hybrid wavelength-division-multiplexed systems, combined source-channel coding using multicarrier modulation or Turbo codes, and performance evaluation of phase-shift-keying and differential-phase-shift-keying signals with nonlinear phase noise.

Han-Wei Cuei is currently a graduate student at the Institute of Communication Engineering of National Taiwan University, Taiwan.